Deng *et al.*
European Journal of Medical Research (2025) 30:463
https://doi.org/10.1186/s40001-025-02716-y

European Journal of Medical Research

RESEARCH Open Access

Endothelial cell iron overload and ferroptosis mediate thrombosis and inflammation through the miR-32-5p/neurofibromin 2 pathway

Ying Deng[1,2†], Xueguang Lin[1,3†], Jun Wei[4†], Bo Chen[1,3†], Huafang Yan[5], Bo Wang[1,3], Jialong Li[1,3], Yuqun Zhao[6], Bo Yu[1,3,7], Jingdong Tang[1,3] and Shuai Jiang[1,3*]

Abstract

Thromboangiitis obliterans (TAO) is characterized by progressive inflammatory vasculopathy featuring thrombotic occlusion. Aberrant thrombosis induces endothelial damage through pathological clotting, while iron may act as a pro-oxidant cofactor. However, the function and mechanism of iron in TAO pathogenesis and endothelial damage remain to be elucidated. In the current study, the iron status and key lipid peroxidation markers (MDA, 4HNE, and ACSL4) were evaluated in patients with TAO and the sodium laurate-induced rat model. The CCK-8 assay, immunofluorescence, western blot, qPCR, and transmission electron microscopy were employed to detect iron overload and ferroptosis in vascular endothelial cells. In addition, bioinformatics analysis, luciferase reporter gene assay, qPCR, and western blot were used to confirm the miR-32-5p/Neurofibromin-2 (NF2) pathway in vitro. The therapeutic feasibility was validated by deferoxamine and Ferrostatin-1 treatment in vivo. The results showed iron overload and increased TFR1 expression in the vessel lesions of patients with TAO, as well as significant increases in MDA, 4HNE, and ACSL4. Serum from patients with TAO increased intracellular iron and lipid peroxidation and decreased the viability of HUVECs in vitro. Mechanism studies indicated that exosomal miR-32-5p increased in patients with TAO and could target and decrease the expression of NF2, which then decreased the phosphorylation of YAP at Ser109 and Ser217 sites. Then the NF2-targeted genes *TFR1* and *ACSL4* were upregulated. Finally, deferoxamine and Ferrostatin-1 treatment relieved the disease score, inflammation, and ferroptosis in vivo. This study newly demonstrates that iron overload and ferroptosis are key risk factors in patients with TAO and that the exosomal miR-32-5p/NF2 pathway may play an important role in TAO pathogenesis.

Keywords Thromboangiitis obliterans, Ferroptosis, Iron metabolism, Neurofibromin 2

[†]Ying Deng, Xueguang Lin, Jun Wei and Bo Chen have contributed equally to this work.

*Correspondence:
Shuai Jiang
zhiyusang@163.com; 14110700053@fudan.edu.cn
Full list of author information is available at the end of the article

Introduction

Thromboangiitis obliterans (TAO), also known as Buerger's disease, is a nonatherosclerotic peripheral vascular disease mediated by immune dysregulation. Clinically, TAO is characterized by obvious thrombosis, occlusion, segmental, and inflammation [1]. As TAO progresses, pain and gangrene can continue to deteriorate, and the amputation rate of patients with 20 years of disease is as high as 46% [2]. Smoking cessation and revascularization surgery can control and relieve the clinical symptoms of such patients [3]. Studies have shown that vascular endothelial cell injury and immune system abnormality are the key risk factors in TAO pathogenesis, but the mechanism remains unclear [4, 5].

Accumulation of iron has been implicated in atherosclerotic and nonatherosclerotic peripheral vascular disease. In cardiovascular diseases, iron overload markedly enhances the thrombosis process via reactive oxygen species and endothelial cell death [6]. Ferroptosis is a form of programmed cell death that is caused by iron overload [7]. In addition to promoting excess free iron, ferroptosis is associated with lipid peroxidation and restricted glutathione peroxidase 4 (GPX4) activity, among others [8, 9]. Iron overload and key ferroptosis-related genes, such as heme oxygenase 1 (HMOX1) and SLC7 A11, are significantly increased in arterial plaques [10, 11]. GPX4 has been shown to be decreased in the severe stage of plaque [12]. Iron restriction and ferroptosis inhibitors could significantly decrease plaque formation [13–15]. The recent studies have shown that malondialdehyde (MDA), Ferritin light chain (FTL), and Ferritin heavy chain 1 (FTH1) are increased in the intestinal tissues of patients with intestinal Behçet's syndrome [16]. Thus, iron metabolism and ferroptosis may play an important role in TAO.

Various regulatory mechanisms of ferroptosis are found in healthy and diseased individuals, among which the Hippo signaling pathway is highly conserved. The Hippo signaling pathway can be activated by neurofibromin-2 (NF2), kidney and brain protein (KIBRA), and G protein receptor [17]. Following Hippo signaling pathway inhibition, the downstream transcriptional regulator YAP/TEAD (transcriptional enhancer associate domain transcription factor) axis controls the transcriptional expression of downstream genes, such as iron long-chain fatty acyl-coenzyme A key genes synthetase 4 (ACSL4) and transferrin receptor 1 (TFR1) [18]. The Hippo pathway also plays an important role in the regulation of vascular homeostasis and the occurrence of arterial diseases. Hippo is involved in the survival, proliferation, migration, and vascular formation of vascular endothelial cells [19]. Hippo pathway activation mediates the expression of endothelial cell adhesion factors and the pro-inflammatory response of immune cells [20].

In the present study, we found disturbed iron homeostasis and ferroptosis signatures in patients with TAO. The results were confirmed in the sodium laurate-induced rat TAO model. We found that the serum-derived exosomal miR32-5p contributed to NF2 pathway inhibition, which then induced iron overload, lipid peroxidation, and ferroptosis in endothelial cells. Iron chelator deferoxamine (DFO) and ferroptosis inhibitor ferrostatin-1 (Fer1) could reduce ferroptosis and alleviate the severity of TAO in vitro and in vivo. Collectively, our results reveal that iron metabolism and ferroptosis are key risk factors and potential new therapy targets for TAO treatment.

Materials and methods

Human study

The study was reviewed and approved by the ethics committee of Shanghai Pudong Hospital, Fudan University Pudong Medical Center (Number: 2022-WZ-23). All methods in this study were conducted under the guidelines and regulations. The TAO patients fulfilled the inclusion criteria as previously described [21]. 47 TAO patients and 37 healthy controls signed written informed consent and the serum samples were collected. The blood vessel tissues (n = 6) were collected after surgery. The healthy controls were sex, age, and smoking habits matched. The general information of all samples was summarized in Table S1.

TAO model

Pathogen-free male Wistar SD rats at 8 weeks old (weighing 220–300 g) were purchased from the Shanghai Laboratory Animal Center (Chinese Academy of Sciences, China). Animals were maintained at the Animal Center of Shanghai Pudong Hospital. All animal experiments were conducted strictly according to the Animal Ethics Committee at the Shanghai Pudong Hospital.

Rats were pre-feeded with a standard AIN-76 A diet or a low-iron diet without iron for 2 weeks (Research Diets, Inc.). The TAO rat model was constructed and modified according to the method reported by Ashida et al. [22]. Briefly, rats were anesthetized and maintained with isoflurane, and the hair of the left hind limbs was removed with depilatory ointment. After disinfecting with betadine, a 2 cm incision was made between the groin and the medial side. The femoral artery was exposed after blunt dissection and the proximal end of the heart was with a hemostatic clamp. Next, 100 μL of sodium laurate (10 mg/mL in ultrapure water adjusted to pH 8.0, Sigma, Shanghai, China) was injected into the distal end of the femoral artery. Then, the clamp was removed after 15

min. Finally, the skin was sutured and betadine was used to prevent infection. For the Sham group, 100 μL saline was injected into the femoral artery, and all other operations were injected with sodium laurate to conduct the TAO model. For treatment, all rats received deferoxamine (DFO, 100 mg/kg, Shanghai, Sigma), Ferrostatin-1 (Fer1, 5 mg/kg, MedChemExpress, Shanghai, China), or saline intraperitoneally every two days after surgery. The femoral artery blood flow was measured using a laser speckle blood flow imaging system (RWD Life Science Co., Ltd., Shenzhen, China) on day 14.

Histology and immunostaining analysis

Human or rat arterial tissues were stained with hematoxylin/eosin or Masson's trichrome staining to assess the pathological changes and the degree of collagen deposition. Perls' staining or DAB-enhanced Perls' staining was performed to assess the iron deposition as previously described [23]. Then, representative sections were incubated with primary antibodies Ferritin (1:1200, ab287968, Abcam), TFR1 (1:400, 54505 s, cell signaling technology), MDA (1:400, ab6464, Abcam), 4HNE (1:50, ab46545, Abcam), ACSL4 (1:600, ab155282, Abcam), 3% hydrogen peroxide, and secondary antibodies following the manufacturer's recommendations. Nikon Eclipse ci-s microscope (Nikon, Badhoevedorp, The Netherlands) was used to assess changes at 100 ×and 200 ×magnification. The average optical density (AOD) of measured by ImageJ v1.54f and Color Deconvolution plugin.

Transmission electron microscope

The rat blood vessels were fixed with a mixture of 2.5% glutaraldehyde for 24 h at 4 °C. The tissues were cut into small pieces (about 1 mm3) and soaked in 1% antimony tetraoxide for 1 h at 4 °C. Then the tissues were dehydrated in acetone and embedded by resin. The embedded resin blocks were cut into ultrathin sections and further stained using uranium acetate and lead citrate. The TEM pictures were taken by transmission electron microscopy (Talos L120 C, Thermo Fisher Scientific).

Cell culture and treatment

Primary human umbilical vein endothelial cells HUVEC were obtained from ATCC. Cells were cultured in Endothelial Cell Medium (ScienCell, USA) and cultured at 37 °C in a 5% CO2 humidified incubator. For TAO serum treatment, cells were starved with fetal bovine serum-free medium for 6 h, the cells were incubated with different concentrations of serum, 300 ng/mL DFO or 1 μM Fer1 were also treated to evaluate the ferroptosis signatures.

For transient transfection assays, cells were seeded in a 12-well plate to ~80% confluence overnight and transfected with negative control or miR-32-5p mimics using RNAimax (Invitrogen, Shanghai, China) following the manufactured instructions. Cell lysates were prepared for mRNA level detection after 24 h transfection and protein levels after 48 h transfection.

Immunocytofluorescence

Cells were cultured in a 12-well plate for 24 h. After different treatment, the cells were cultured with 1 μM FerroOrange (DOJINDO LABORATORISE, Shanghai, China) for 1 h or 5 μM Liperfluo (DOJINDO LABORATORISE, Shanghai, China) for 5 h. When incubation with a fluorescent probe was completed, cells were washed with cold 1× PBS three times. Super-resolution confocal microscope Zeiss-LSM880 with Airyscan (Zeiss, Germany) was used to assess immunofluorescence staining.

Tissue malondialdehyde (MDA) assay

The level of MDA was measured by using a malondialdehyde assay kit (Nanjing Jiancheng Bioengineering Institute, Nanjing, China). Briefly, tissues were homogenized and 0.1 mL lysates were incubated with thiobarbituric acid and glacial acetic acid in a 95 ℃ water bath for 40 min. After cooling down to room temperature, samples were centrifuged for 10 min at 4000 rpm. Then the optical density (OD) values of 0.25 mL supernates were detected at 532 nm. The MDA level was calculated by converting it to the standard sample. The total protein level of samples was measured by the Lowry protein assay kit (Sangon Biotech, Shanghai, China).

Immunocytochemistry

The cells were seeded in a 12-well plate and after treatment, cells were incubated with 20 μM Lpierfluo (DOJINDO, Shanghai, China) for 3 h or 1 μM FerroOrange (DOJINDO, Shanghai, China) for 1 h. Then, the cells were washed with PBS and fixed with 4% paraformaldehyde for 15 s. The fluorescence was observed with a super-resolution confocal microscope Zeiss-LSM880 with Airyscan (Zeiss, Germany).

RT-PCR and quantitative RT-PCR analysis

Total RNA from HUVEC and rats' femoral artery tissues were extracted using Trizol (Invitrogen, Carlsbad, CA, USA), and then cDNA was synthesized by using the RevertAid First Strand cDNA Synthesis Kit (Thermo Fisher, Shanghai, China) according to the instructions of the manufacturer. The specific primers for each gene were designed using Primer 6 and synthesized by General Biotech Co., Ltd. (Shanghai, China). The RT-PCR amplification was conducted using the SYBR Green I PCR Kit (TaKaRa, Shanghai, Japan) according to the manufacturer's instructions. The reaction was carried out on Applied

Biosystems™ Q7 (Applied Biosystems). RT-PCR conditions were 95 °C for 5 min, followed by 40 cycles of 95 °C for 15 s, 60 °C for 45 s, and the conditions for getting the dissociation curve were 95 °C for 15 s, 60 °C for 15 s, 95 °C for 15 s. For each sample, the relative gene expression was calculated using a relative ratio to β-actin. Related RT-PCR primers can be found in Table S2.

Western blot

Cell lysates extracted from cultured cells were used for subsequent immunoblot analyses. The total protein concentration was measured using the Lowry protein assay kit. Equal amounts of protein from each sample were subjected to 10% SDS PAGE gel electrophoresis after which protein was transferred to PVDF membranes (Millipore, Billerica, MA, USA). Membranes were blocked in 5% BSA in TBST at room temperature for 1 h after which they were incubated with primary antibodies or internal control β-actin (1:5000) at 4 °C overnight. Membranes were washed three times with TBST for a total of 30 min and then incubated with the horseradish peroxidase-conjugated secondary antibody of goat antirabbit, or goat antimouse lgG for 2 h at room temperature. The protein bands were visualized with an ECL solution.

Exosome extraction and miR-32-5p expression level validation

Exosomes were extracted from serum by TransExo Serum/Plasma Exosome Kit (TransGen Biotech, Beijing, China). Briefly, serum samples were centrifuged with 3000 ×g to remove the precipitate. Then samples were incubated with exosome precipitation solution for 30 min and centrifuged with 10,000 ×g for 10 min. The exosomes were enriched and purified with exosome resuspension solution and exosome microsphere beads. For miR-32-5p expression level measurement, total RNA from exosomes was reversed and transcribed to cDNA with miRNA 1 st strand cDNA synthesis kit (Takara, Dalian, China). Then the level of miR-32-5p was quantified by QPCR.

Luciferase report assay

The full-length 3' UTR of NF2 was inserted into the plasmid containing luciferase. Then miR-32-5p mimics or negative control was transfected into HUVECs together with pRL-SV40 and NF2 plasmid. Twenty-four hours later, a dual-luciferase activity assay was performed according to the standard protocol.

Power calculations

The data are expressed as mean ± SEM. Either an independent two-group *t* test or one-way ANOVA test with post hoc LSD's multiple comparison test was used for the evaluation of significance between different groups. A *P* value of less than 0.05 was considered statistically significant.

Results

Patients with TAO exhibit iron overload and excess lipid peroxidation

To explore the signatures of iron metabolism in patients with TAO, serum from 47 patients and 37 matched controls were collected to evaluate iron parameters. The included patients were male, the mean age was 45.41 ± 9.72, 93.62% had smoking habits, while the control group was matched by age, sex, and smoking habits (Table S1). In patients with TAO, the serum iron (SI) level and the total iron-binding-capability (TIBC) significantly decreased, with no significant difference in unsaturated iron-binding capacity (UIBC) and a decrease in transferrin saturation (TS) level (Figure S1a–d). These results indicate defects in iron utilization in the circulation of patients with TAO due to inflammation or chronic infection. Therefore, we next sought to evaluate the iron levels in arterial lesions and adjacent normal arteries using the DAB-enhanced Perls' stain and the Ferritin protein level. As expected, the arterial lesions showed abnormal hyperplasia (Figure S1f), together with significantly increased iron levels in endothelial and vascular smooth muscle cells of patients with TAO. Moreover, TFR1, a marker of iron absorption and ferroptosis protein, increased in the vascular lesions, especially in vascular endothelial cells (Fig. 1a, c). As iron overload could increase lipid peroxidation via the Fenton reaction, we found that MDA, 4HNE, and ACSL4 increased in the vascular lesion, both in vascular endothelial cells and vascular smooth muscle cells (Fig. 1b, d). The serum MDA level also increased in patients with TAO (Figure S1e). These results reveal iron overload and lipid peroxidation in damaged vascular lesions in TAO.

Serum of patients with TAO induces ferroptosis in vascular endothelial cells

Vascular endothelial cells, as the primary effector cells at the blood–tissue interface, respond to circulatory stimuli and drive disease progression. We first explored the effects of serum on vascular endothelial cells. As shown in Fig. 2a, cell viability was significantly and dose-dependently decreased by the serum of patients with TAO, but not by the serum of healthy controls or fetal bovine serum (FBS). The serum of patients with TAO increased the expression of genes related to iron overload and ferroptosis, such as FTH1, FTL, TFR1, and ACSL4 (Fig. 2b). Moreover, cell viability could be reversed by DFO and Fer1 (Fig. 2c). Mechanism studies showed that the serum

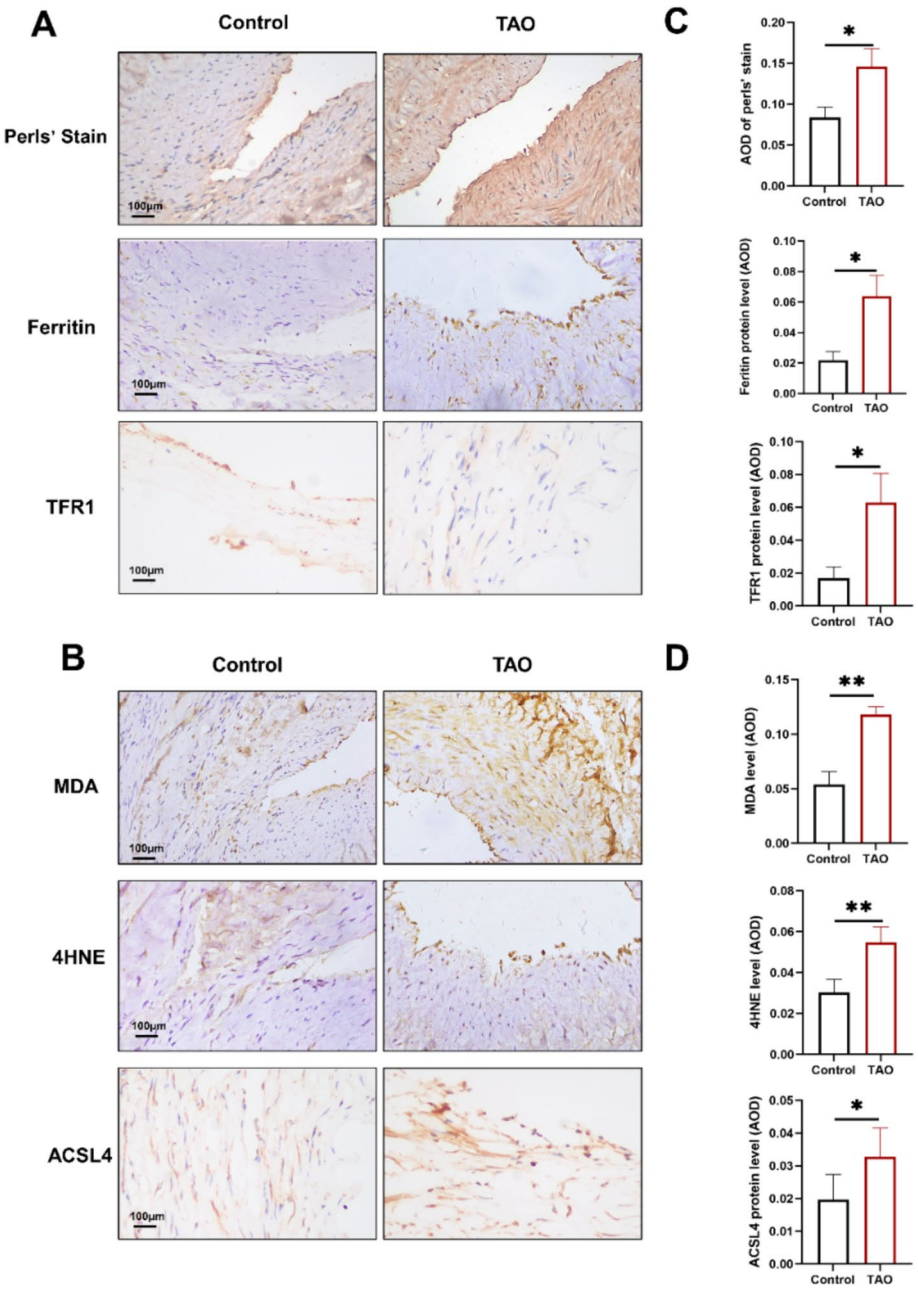

Fig. 1 The level of key iron parameters and lipid peroxidation markers in blood vessel tissues of TAO patients. The blood vessel tissues after surgery were performed with IHC to evaluate the level of **a** iron levels by DAB enhanced perls' stain (upper), Ferritin protein level to indicate the iron storage level (middle), and TFR1 protein level (lower) (n = 6). Then, the lipid peroxidation levels were indicated by IHC stain of **b** MDA (upper), 4HNE (middle), and ACSL4 (lower) in the vascular tissues (n = 6). The IHC results were semiquantitative by ImageJ software **c**, **d**. *T* test, *showed compassion between the control group and the disease groups. *: P < 0.05; **: P < 0.01, ***: P < 0.001, Error bar means SEM

of patients with TAO significantly increased the protein levels of Ferritin, ACSL4, and TFR1, all of which are downstream targeted genes of NF2. As expected, NF2 was downregulated, together with decreased phosphorylation of YAP at Ser109 and Ser217 sites (Fig. 2d, e). The immunofluorescent results also confirmed that the serum of patients with TAO increased intracellular Fe^{2+} and lipid reactive oxygen species levels, which could be relieved by DFO and Fer1 (Fig. 2f). NF2 is an upstream regulator of ferroptosis, whose inhibition could promote the expression of TFR1 and ACSL4. As expected, the mRNA and protein levels of NF2 significantly decreased

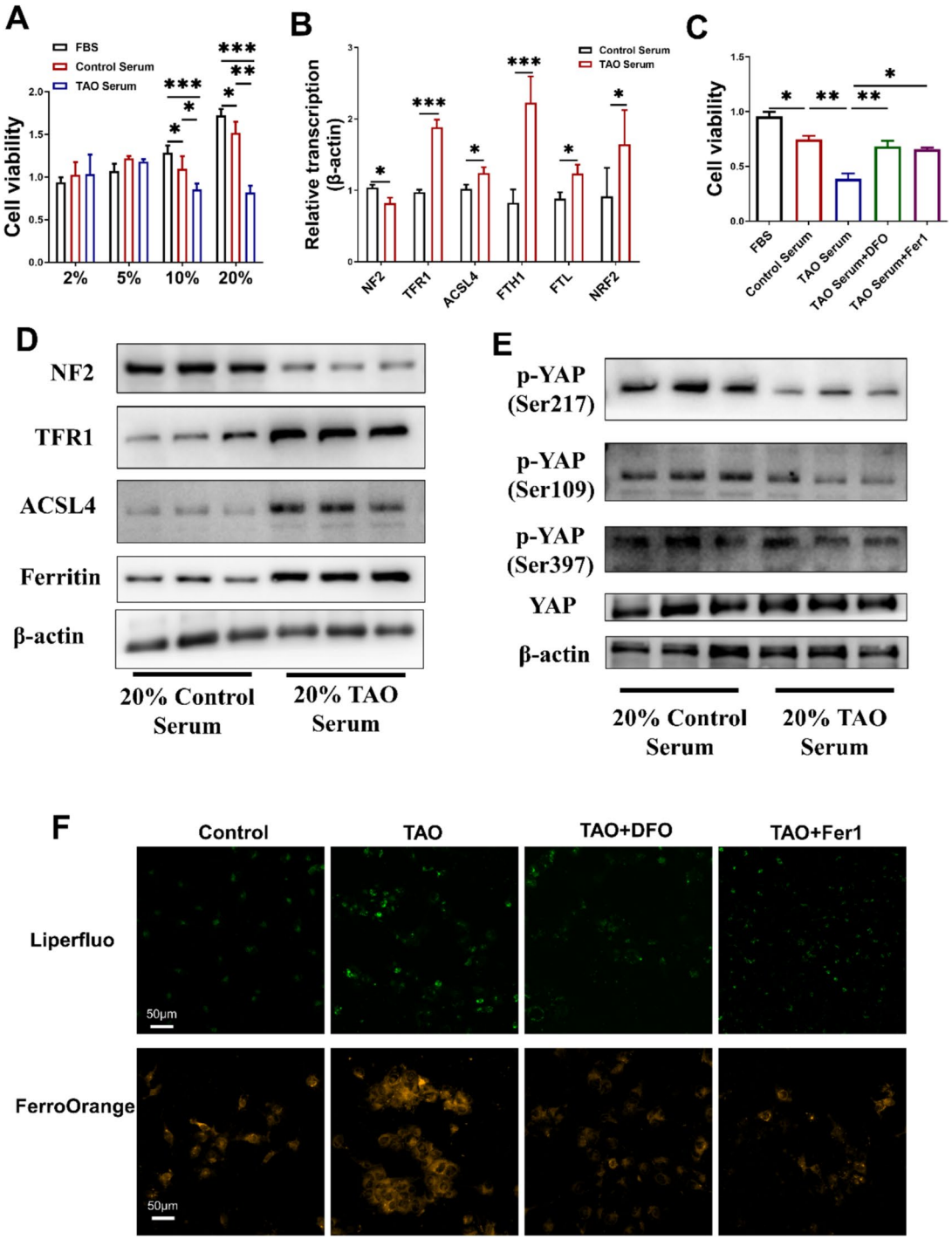

Fig. 2 Ferroptosis was induced after the serum of the TAO patient's treatment. **a** The cell viability of HUVEC cells after FBS, control serum, or TAO serum treatment (n = 5). **b** mRNA levels of key iron and ferroptosis-related markers after treatment with serum from control or TAO patients (n = 3). **c** Cell viability evaluated the capability of DFO and Fer1 after TAO serum treatment (n = 5). Protein levels of key iron, ferroptosis-related markers **d**, and NF2-YAP pathway **e** after treatment with serum from control or TAO patients (n = 3). **f** Then, the cellular iron and lipid peroxidation levels after serum treatment. *showed compassion between the control group and disease groups (n = 3). *T* test or one-way ANOVA, *: $P < 0.05$; **: $P < 0.01$, ***: $P < 0.001$, Error bar means SEM

after the addition of serum from a patient with TAO (Fig. 2c, d). These results indicate that endothelial cell ferroptosis is invoked in patients with TAO, which is related to the NF2 pathway.

Exosomal miR-32-5p is involved in ferroptosis via NF2 depression in TAO

Exosomes serve as pivotal mediators of intercellular communication within the circulatory system. We screened all of the differentially expressed exosomal miRNAs in patients with TAO as we previously reported [24]. Bioinformatics prediction via miRDB, miRWalk, miRMap, TargetScan, and TARbase databases revealed that miR-32-5p was an upregulated microRNA that could target NF2 (Fig. 3a, b). First, we confirmed that the level of exosomal miR-32-5p significantly increased in exosomes from patients with TAO (Figs. 3c and S2). The results of the dual-luciferase reporter assay indicated that miR-32-5p mimics could decrease the activity of NF2 (Fig. 3d). Transfection of the miR-32-5p mimics significantly inhibited the mRNA and protein levels of NF2 (Fig. 3e, f). Moreover, miR-32-5p increased the mRNA and protein levels of TFR1 and ACSL4, which decreased DFO and Fer1 treatment (Fig. 3g). The intracellular iron and lipid peroxidation levels increased after miR-32-5p transfection and were downregulated by DFO and Fer1 (Fig. 3i). The above-mentioned results suggest that exosomal miR-32-5p represents a key regulator in patients with TAO by targeting NF2.

DFO and Fer1 alleviate the severity of sodium laurate-induced TAO in rats

To ascertain whether DFO and Fer1 are effective in treating TAO, the SD rat TAO model was induced by sodium laurate. Briefly, DFO or Fer1 was administered once every 2 days, starting 7 days before model construction (Fig. 4a). We observed weight loss in the TAO group on day 2, while DFO and Fer1 treatment caused the weight to be regained after 6 days (Fig. 4b). The typical signs of ischemia and gangrene were seen in the TAO group, with significant improvement of symptoms in the DFO and Fer1 treatment groups (Fig. 4c, d). The HE staining results showed that the femoral arteries in the TAO group had massive infiltration of red blood cells and lymphocytes, as well as increased permeability of the vascular endothelial cell layer, while the DFO and Fer1 treatment groups had little cell infiltration and regulated structural integrity (Fig. 4e). Masson's staining revealed thrombosis and extensive extracellular matrix (ECM) accumulation in arteries, with relatively less ECM deposition among the arteries in the DFO and Fer1 treatment groups (Fig. 4f). Consistent with the pathological changes, DFO and Fer1 could significantly decrease the disease score (Figure S3a). Furthermore, DFO and Fer1 significantly depressed the inflammatory process by decreasing the mRNA levels of *Il-1β, IL-6, TNFα,* and *Ifn-γ* (Figure S3b). The mRNA levels of *Icam1, Vcam1, tPa,* and *Pai-1* also decreased in the DFO and Fer1 groups, indicating that endothelial cell activation and thrombosis were also refined by treatment (Figure S3c). These results indicate that DFO and Fer1 protect against sodium laurate-induced TAO.

DFO and Fer1 protect against TAO by iron chelation and antiferroptosis properties

We next sought to further identify the role of disrupted iron metabolism and ferroptosis in the pathogenesis of TAO. The results of the iron assay showed that the iron content of femoral artery tissues was 3.61 times higher in the TAO group than in the control group (Fig. 5a). The levels of mRNA associated with iron deposition (*Fth1*, *Ftl*) and iron absorption (*Dmt1*, *Tfr1*) significantly increased in the arteries of the TAO group (Fig. 5b). The Perls' stain, IHC of TFR1and Ferritin protein levels were also confirmed iron overload in the TAO group, which was relieved by DFO and Fer1 (Figs. 5c and S3D), while the iron parameters in the serum of rats showed minor changes (Figure S3e–g). Next, we found that the excessive lipid peroxidation accumulation and the levels of MDA, 4HNE, and ACSL4 in artery tissues were significantly higher in the TAO model group (Fig. 5c, d). More importantly, the mitochondrial morphology was abnormal in the TAO group (i.e., shrunken, increased membrane density, and reduced mitochondrial cristae), while these phenotypes were mitigated by DFO or Fer1 treatment (Fig. 5e). The lipid peroxidation and ferroptosis-related genes were also inhibited by DFO and Fer1 treatment (Fig. 5f). These results further confirm that NF2 signaling is depressed in TAO, while iron chelation and ferroptosis inhibition represent novel approaches to TAO treatment.

Discussion

Vasculitis encompasses a variety of diseases characterized by inflammation, immune dysfunction, and blood vessel involvement [25, 26]. TAO is an ideal vasculitis disease model driven by excessive inflammation and thrombosis [27, 28]. However, not much is known about the mechanism and treatment of TAO, and the only symptomatic treatments include smoking cessation, therapies for rest pain, and healing ischemic ulcers [29–31]. Here, we reveal for the first time the presence of iron overload in lesions of patients with TAO and in a rat model of TAO. We also observed ferroptosis signatures in serum and lesions. Functional studies revealed that miR-32-5p/NF2 signaling was depressed in TAO. Treatment with DFO and Fer1 alleviated TAO by iron chelation and ferroptosis inhibition (Fig. 6). Our study highlights the critical role

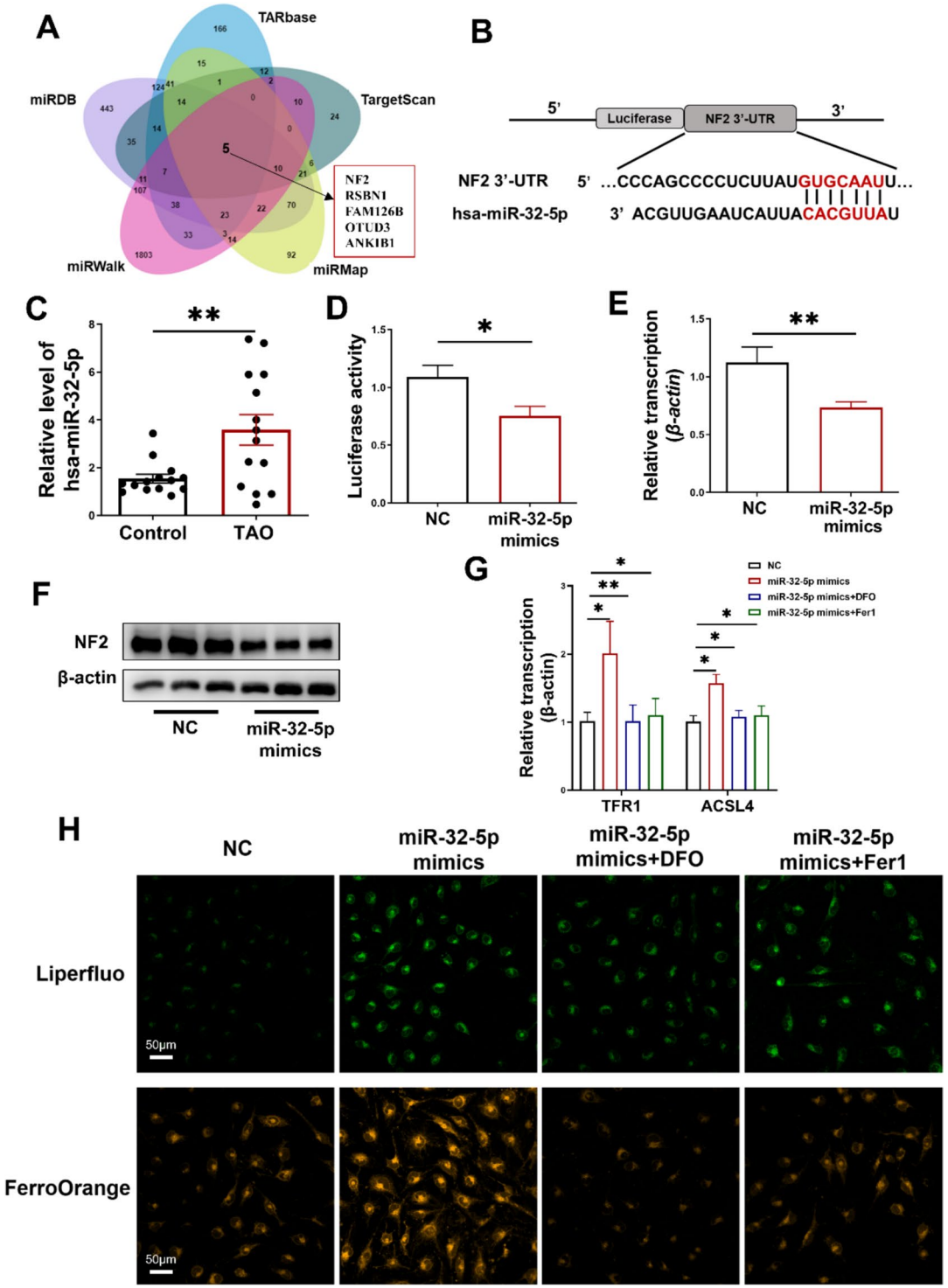

Fig. 3 A high level of exosomal miR-32-5p was involved in ferroptosis by binding to NF2. **a**, **b** Interaction of prediction between miR-32-5p and NF2. **c** The level of miR-32-5p in serum-derived exosomes from 15 controls and 15 TAO patients. **d** Luciferase activities of NF2 after miR-32-5p mimic transfection. **e** mRNA and **f** protein level of NF2 after miR-32-5p transfection (n = 3). **g** mRNA level of TFR1, ACSL4 after miR-32-5p transfection (n = 3). **h** Intracellular Fe^{2+} and lipid peroxidation levels in HUVEC cells after miR-32-5p transfection, DFO, or Fer1 treatment (n = 3). *T* test or one-way ANOVA, *showed compassion between the control group and the disease groups. *: P < 0.05; **: P < 0.01, ***: P < 0.001, Error bar means SEM

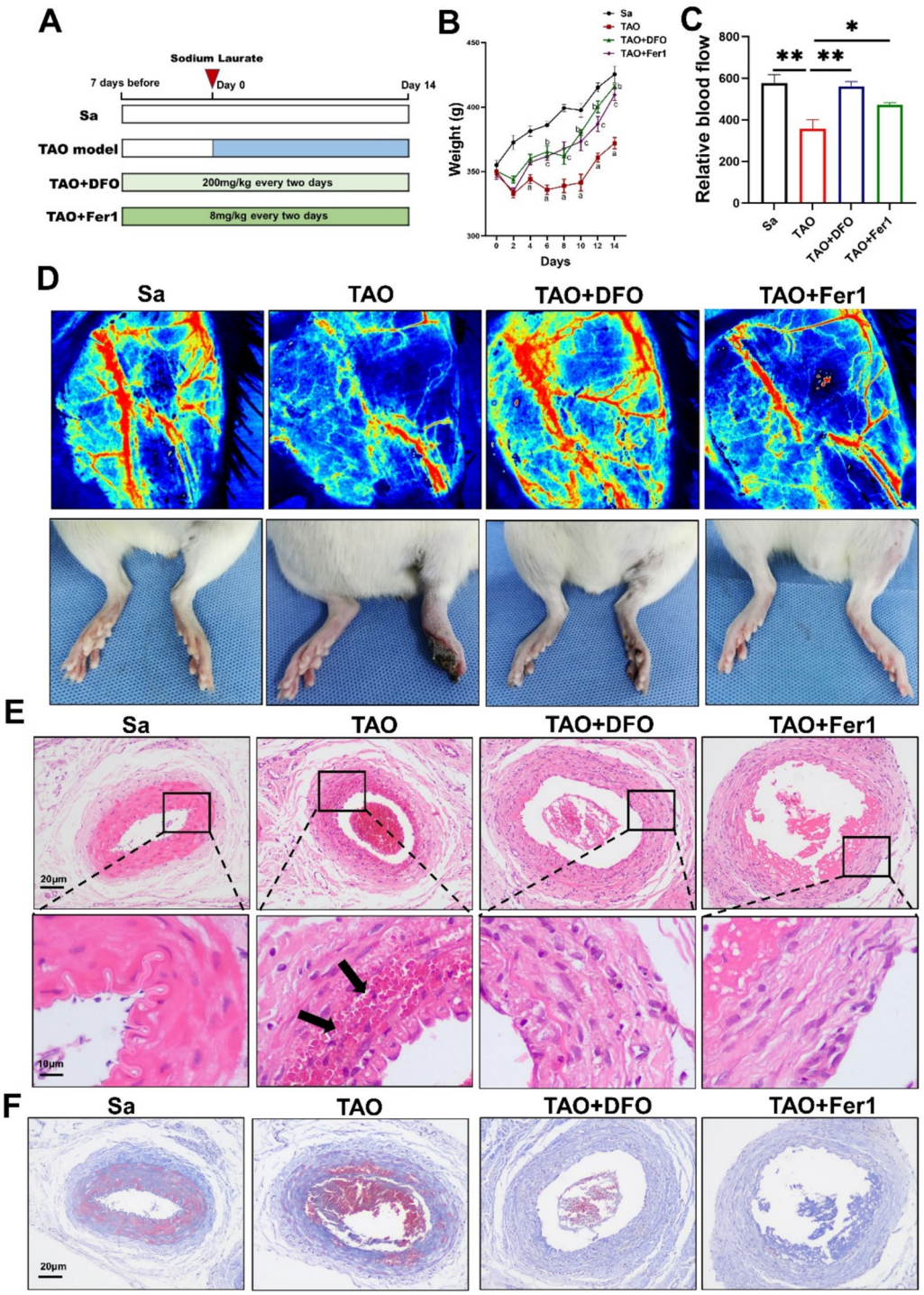

Fig. 4 DFO and Fer1 improved clinical symptoms, inflammation, and thrombosis in the rat TAO model. **a** The schedule of rat TAO model introduction and treatments. DFO and Fer1 were treated from 7 days before sodium laurate injection to the endpoint of the model. **b** The curve of rat weight during the TAO process (n = 7). **c** The level of relative blood flow of the femoral arteries in different groups (n = 7). **d** The representative images of blood flow and tissue gangrene on the 14 th day after sodium laurate injection (n = 3). Then the tissues were evaluated by (E) HE (100 ×) and (F) Masson staining (100 ×) of femoral arteries in the rat TAO model, the black arrows showed infiltration of red cells and lymphocytes. n = 7. *T* test or one-way ANOVA, * showed compassion between the control group and the disease groups. *: $P < 0.05$; **: $P < 0.01$, ***: $P < 0.001$, Error bar means SEM

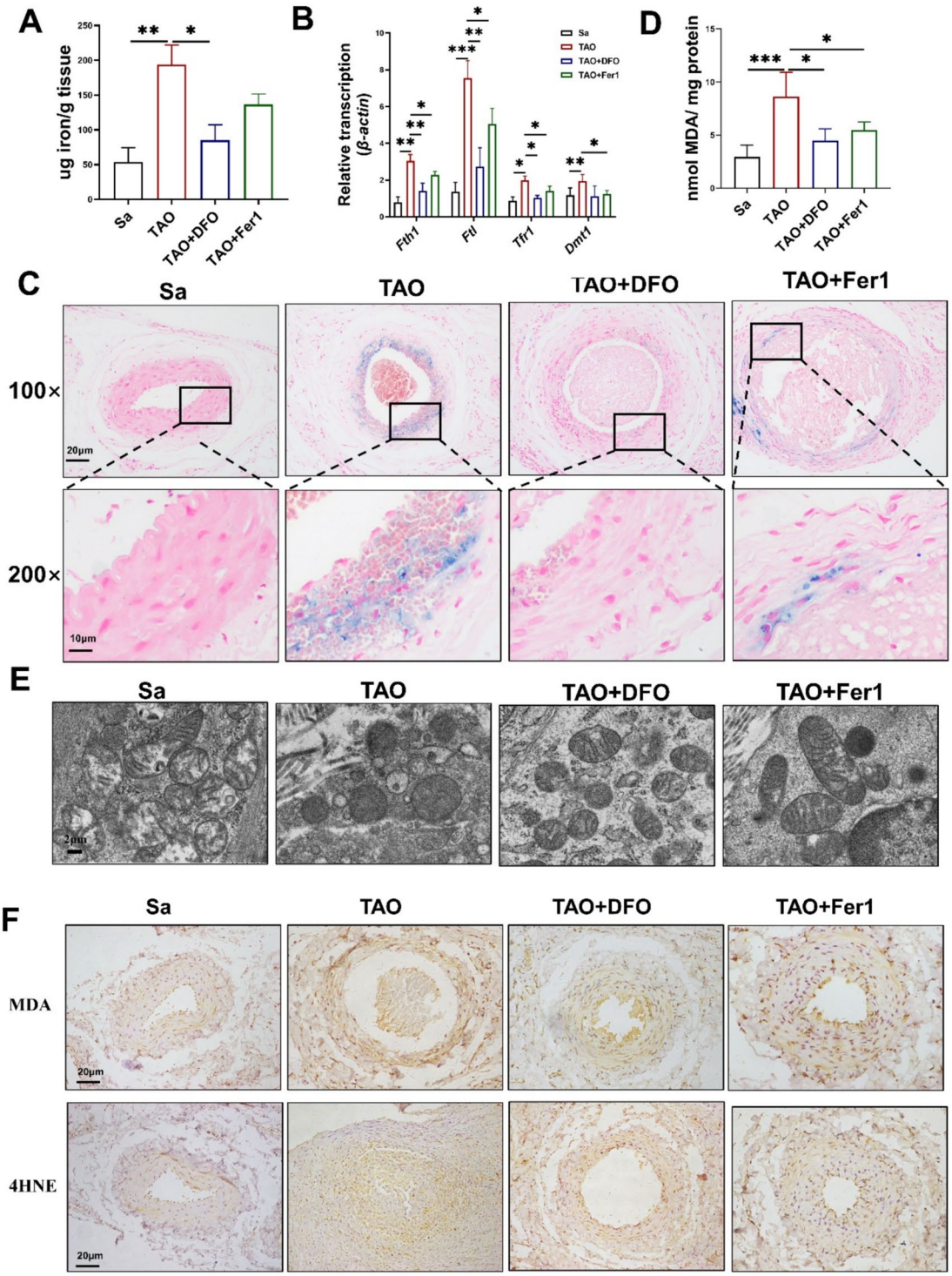

Fig. 5 DFO and Fer1 balanced iron metabolism and inhibited ferroptosis in the rat TAO model. **a** Iron levels of femoral arterial lesions in the rat TAO model (n = 7). **b** The mRNA level of iron related genes in femoral arterial lesions of the rat TAO model (n = 7). **c** Perls' stain (200 ×) in arterial tissues (n = 7). **d** The MDA level of femoral arteries among different groups (n = 7). **e** TEM images showed mitochondrial morphology in tissues (n = 3). Finally, the levels of **f** MDA and 4HNE were measured. n = 7. one-way ANOVA, * showed compassion between the control group and the disease groups. *: P < 0.05; **: P < 0.01, ***: P < 0.001, Error bar means SEM

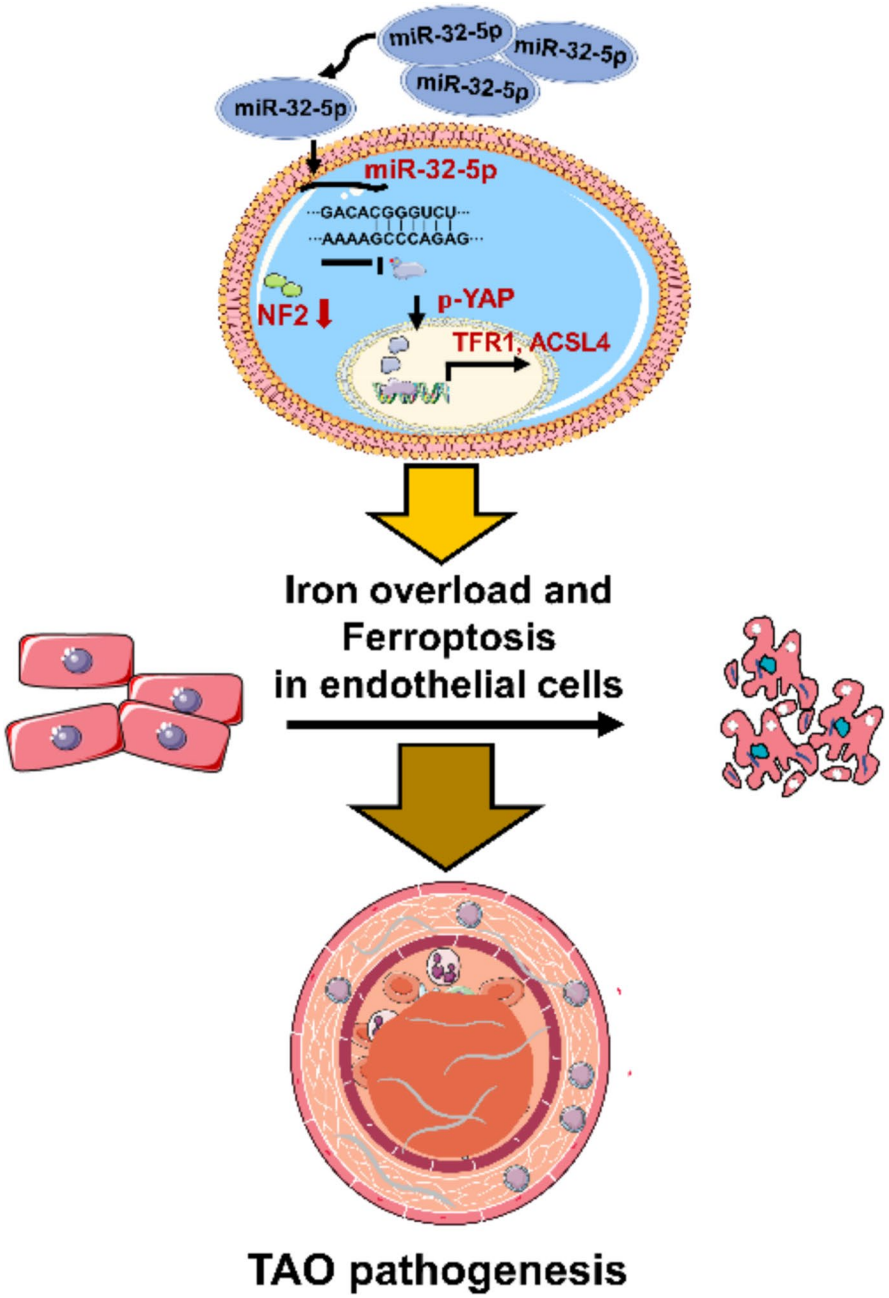

Fig. 6 Mechanism hypothesis of exosomal miR-32-5p in the pathogenesis of TAO. miR-32-5p was upregulated in the serum of TAO patients. miR-32-5p targeted NF2 and decreased the level of p-YAP. The increased expression of NF2 downstream genes TFR1 and ACSL4 promoted endothelial iron overload and ferroptosis. Endothelial cell ferroptosis led to the progression of TAO

of iron overload and ferroptosis in the pathology of TAO, suggesting that targeting iron metabolism and ferroptosis may serve as potential therapeutic strategies.

Iron is an essential trace element that plays an important role in normal physiological regulation, oxidative stress, ferroptosis, and so on. Iron-mediated ferroptosis could be a major factor in many cardiovascular diseases such as ischemic reperfusion injury and atherosclerosis [30, 31]. By evaluating the iron metabolism and ferroptosis signatures in clinical samples and a rat TAO model, we found that the serum iron, total iron binding capability, and transferrin saturation significantly decreased in patients with TAO, indicating the existence of chronic infection and inflammation [32].

Abnormal production of reactive oxygen species has been reported in TAO [28]. The levels of NADPH oxidase and oxidized low-density lipoprotein have been shown to be positively associated with disease severity [33]. Oxidative stress can activate the NFκB-INOS-NO signaling pathway in vascular endothelial cells, leading to excessive superoxide anion to promote lipid peroxidation and directly induce endothelial cell damage [34]. In addition, sodium laurate has been shown to induce rat TAO following local injection into the femoral artery; the model partially mimics the associated pathological changes, including inflammation, endothelial injury, and thrombosis [22]. In our study, we found that excessive iron overload and lipid peroxidation were involved in the tissue lesions of patients with TAO and the rat TAO model. The key ferroptosis-related markers TFR1 and ACSL4 were significantly accumulated in TAO. TFR1 is a specific ferroptosis marker that promotes intracellular iron overload [35], while ACSL4 increases sensitivity to ferroptosis by promoting polyunsaturated long-chain fatty acid metabolism [36]. Both TFR1 and ACSL4 are downstream target genes of the NF2/Hippo pathway [37]. Consequently, we revealed that NF2 is also downregulated in TAO. These results confirm that iron overload and ferroptosis represent a novel signature in TAO that is involved in chronic infection, inflammation, and lipid peroxidation.

Our previous studies have shown multiple differentially enriched serum-derived exosomal miRNAs in patients with TAO, which may represent a marker of disease or cell death [24]. We confirmed that exosomes could induce cell ferroptosis, while the cell death was rescued by DFO and Fer1. Through bioinformatics prediction and functional validation, miR-32-5p was found to be increased in exosomes from patients with TAO. The high level of miR-32-5p depressed the expression of NF2 and then induced ferroptosis. Several reports have indicated that miR-32-5p is involved in epithelial or endothelial injury [38, 39]. Moreover, upregulated miR-32-5p weakens cell proliferation in several cancers [40]. For the first time, we report that miR-32-5p represents a biomarker in TAO and is involved in ferroptosis by targeting the NF2/Hippo pathway.

Despite the strengths of our study, some limitations remain to be addressed in future studies. First, as TAO is a complex disease with great heterogeneity, large clinical size, and stratified analysis should be performed. Second, our study focused on vascular endothelial cell damage in TAO, and the role of iron hemostasis and ferroptosis signatures in other cells, such as immune and vascular smooth muscle cells, remains to be explored. Third, although DFO and Fer1 could relieve disease severity, the thrombus and tissue damage still existed. Combined treatment with DFO, Fer1, and other antithrombotic therapies may be a better choice than traditional treatment such as smoking cessation. Finally, we only studied the role of the miR-32-5p/NF2 axis, and the detailed mechanism of downstream target regulation (TFR1, ACSL4) remains to be defined in the future.

In conclusion, these results highlight the critical role of iron and ferroptosis in TAO pathogenesis. Serum-derived exosomal miR-32-5p is involved in iron overload and ferroptosis by targeting NF2. Treatment with DFO or Fer1 significantly relieves the clinical symptoms, as well as inflammation, fibrosis, iron overload, and ferroptosis. Targeting iron metabolism and ferroptosis represents a convincing strategy to cure vasculitis such as TAO.

Supplementary Information

The online version contains supplementary material available at https://doi.org/10.1186/s40001-025-02716-y.

Additional file 1

Additional file 2

Acknowledgements

The study was supported by Funded by the Young Medical Talents Training Program of Pudong Health Committee of Shanghai (PWRq2023-19), the Elite Talent Program of Pudong Municipal Commission of Health Committee of Shanghai (2025PDWSYCQN-05), the Research Grant for Health Science and Technology of Pudong Municipal Commission of Health Committee of Shanghai (PW2022 A-30), the Research Grant for Health Science and Technology of Pudong Municipal Commission of Health Committee of Shanghai (PKJ2023-Y04). The Key Disciplines Construction Project of Pudong Local Health Commission of Shanghai (PWZxk2022-01). The clinical medicine New Quality Specialty of Pudong Local Health Commission of Shanghai (2024-PWXZ-11). We thank LetPub (www.letpub.com.cn) for its linguistic assistance during the preparation of this manuscript.

Author contributions

Conceptualization: Jingdong Tang, Bo Yu, and Shuai Jiang; Methodology: Ying Deng, Bo Chen, and Xueguang Lin; Formal analysis and investigation: Jun Wei; Writing—original draft preparation: Shuai Jiang, Jialong Li; Writing—review and editing: Jingdong Tang; Funding acquisition: Ying Deng, Jingdong Tang, and Shuai Jiang; Resources: Yuqun Zhao, Bo Wang, and Huafang Yan; Supervision: Jingdong Tang. All authors read and approved the final manuscript.

Data availability

Data is provided within the manuscript or supplementary information files.

Declarations

Competing interests

The authors declare no competing interests.

Author details

[1]Department of General Surgery, Shanghai Pudong Hospital, Fudan University Pudong Medical Center, Shanghai Key Laboratory of Vascular Lesions Regulation and Remodeling, Shanghai 201399, China. [2]Fudan Zhangjiang Institute, Shanghai, China. [3]Center for Medical Research and Innovation, Shanghai Pudong Hospital, Fudan University Pudong Medical Center, Shanghai 201399, China. [4]Southern Medical University Affiliated Fengxian Hospital, Shanghai, China. [5]Physical Examination Center, Shanghai Pudong Hospital, Fudan

University Pudong Medical Center, Shanghai, China. [6]Shan Xi Yi Kang Vasculitis Hospital, Taiyuan, Shanxi, China. [7]Department of Vascular Surgery, Huashan Hospital, Fudan University, Shanghai, China.

Received: 5 April 2025 Accepted: 21 May 2025
Published online: 06 June 2025

References

1. Olin JW. Thromboangiitis obliterans. Curr Opin Rheumatol. 1994;6:44–9.
2. Piazza G, Creager MA. Thromboangiitis obliterans. Circulation. 2010;121:1858–61.
3. Hurt RD, Hays JT. Urinary tobacco alkaloid measurement in patients having thromboangiitis obliterans. Mayo Clin Proc. 2008;83:1187–8.
4. Halacheva K, Gulubova MV, Manolova I, Petkov D. Expression of ICAM-1, VCAM-1, E-selectin and TNF-alpha on the endothelium of femoral and iliac arteries in thromboangiitis obliterans. Acta Histochem. 2002;104:177–84.
5. Leu HJ. Early inflammatory changes in thromboangiitis obliterans. Pathol Microbiol (Basel). 1975;43:151–6.
6. Franchini M, Targher G, Montagnana M, Lippi G. Iron and thrombosis. Ann Hematol. 2008;87:167–73.
7. Dixon SJ, Lemberg KM, Lamprecht MR, Skouta R, Zaitsev EM, Gleason CE, Patel DN, Bauer AJ, Cantley AM, Yang WS, et al. Ferroptosis: an iron-dependent form of nonapoptotic cell death. Cell. 2012;149:1060–72.
8. Stockwell BR, Friedmann Angeli JP, Bayir H, Bush AI, Conrad M, Dixon SJ, Fulda S, Gascón S, Hatzios SK, Kagan VE, et al. Ferroptosis: a regulated cell death nexus linking metabolism, redox biology, and disease. Cell. 2017;171:273–85.
9. Stockwell BR. Ferroptosis turns 10: emerging mechanisms, physiological functions, and therapeutic applications. Cell. 2022;185:2401–21.
10. Fang X, Ardehali H, Min J, Wang F. The molecular and metabolic landscape of iron and ferroptosis in cardiovascular disease. Nat Rev Cardiol. 2023;20:7–23.
11. Zhang X, Zheng C, Gao Z, Chen H, Li K, Wang L, Zheng Y, Li C, Zhang H, Gong M, et al. SLC7A11/xCT prevents cardiac hypertrophy by inhibiting ferroptosis. Cardiovasc Drugs Ther. 2022;36:437–47.
12. Zhou Y, Zhou H, Hua L, Hou C, Jia Q, Chen J, Zhang S, Wang Y, He S, Jia E. Verification of ferroptosis and pyroptosis and identification of PTGS2 as the hub gene in human coronary artery atherosclerosis. Free Radic Biol Med. 2021;171:55–68.
13. Lee TS, Shiao MS, Pan CC, Chau LY. Iron-deficient diet reduces atherosclerotic lesions in apoE-deficient mice. Circulation. 1999;99:1222–9.
14. Minqin R, Rajendran R, Pan N, Tan BK, Ong WY, Watt F, Halliwell B. The iron chelator desferrioxamine inhibits atherosclerotic lesion development and decreases lesion iron concentrations in the cholesterol-fed rabbit. Free Radic Biol Med. 2005;38:1206–11.
15. Zhang WJ, Wei H, Frei B. The iron chelator, desferrioxamine, reduces inflammation and atherosclerotic lesion development in experimental mice. Exp Biol Med (Maywood). 2010;235:633–41.
16. Hou CC, Bao HF, She CH, Chen HY, Pan GX, Chen HN, Rui HB, Guan JL. miR-141-3p attenuates RSL3-induced ferroptosis and intestinal epithelial-mesenchymal transition via directly inhabits ZEB1 in intestinal Behçet's syndrome. Clin Rheumatol. 2024;43:2273–85.
17. Segrelles C, Paramio JM, Lorz C. The transcriptional co-activator YAP: a new player in head and neck cancer. Oral Oncol. 2018;86:25–32.
18. Yu FX, Zhao B, Panupinthu N, Jewell JL, Lian I, Wang LH, Zhao J, Yuan H, Tumaneng K, Li H, et al. Regulation of the Hippo-YAP pathway by G-protein-coupled receptor signaling. Cell. 2012;150:780–91.
19. He J, Bao Q, Yan M, Liang J, Zhu Y, Wang C, Ai D. The role of Hippo/yes-associated protein signalling in vascular remodelling associated with cardiovascular disease. Br J Pharmacol. 2018;175:1354–61.
20. Yamashiro Y, Thang BQ, Ramirez K, Shin SJ, Kohata T, Ohata S, Nguyen TAV, Ohtsuki S, Nagayama K, Yanagisawa H. Matrix mechanotransduction mediated by thrombospondin-1/integrin/YAP in the vascular remodeling. Proc Natl Acad Sci USA. 2020;117:9896–905.
21. Tang J, Gan S, Zheng M, Jiang Y, Feng Y, Miao J. Efficacy of endovascular radiofrequency ablation for thromboangiitis obliterans (Buerger's disease). Ann Vasc Surg. 2017;42:78–83.
22. Ashida S, Ishihara M, Ogawa H, Abiko Y. Protective effect of ticlopidine on experimentally induced peripheral arterial occlusive disease in rats. Thromb Res. 1980;18:55–67.
23. Guo S, Jiang S, Epperla N, Ma Y, Maadooliat M, Ye Z, Olson B, Wang M, Kitchner T, Joyce J, et al. A gene-based recessive diplotype exome scan discovers FGF6, a novel hepcidin-regulating iron-metabolism gene. Blood. 2019;133:1888–98.
24. Deng Y, Tong J, Shi W, Tian Z, Yu B, Tang J. Thromboangiitis obliterans plasma-derived exosomal miR-223-5p inhibits cell viability and promotes cell apoptosis of human vascular smooth muscle cells by targeting VCAM1. Ann Med. 2021;53:1129–41.
25. Sims C, Clowse MEB. A comprehensive guide for managing the reproductive health of patients with vasculitis. Nat Rev Rheumatol. 2022;18:711–23.
26. Aymonnier K, Amsler J, Lamprecht P, Salama A, Witko-Sarsat V. The neutrophil: a key resourceful agent in immune-mediated vasculitis. Immunol Rev. 2022;314(1):326–56.
27. Cooper LT, Tse TS, Mikhail MA, McBane RD, Stanson AW, Ballman KV. Long-term survival and amputation risk in thromboangiitis obliterans (Buerger's disease). J Am Coll Cardiol. 2004;44:2410–1.
28. Shyy JY, Chien S. Role of integrins in endothelial mechanosensing of shear stress. Circ Res. 2002;91:769–75.
29. Cacione DG, Macedo CR, do Carmo Novaes F, Baptista-Silva JC. Pharmacological treatment for Buerger's disease. Cochrane Database Syst Rev. 2020;5:Cd011033.
30. Dong Z, Pan T, Fang Y, Wei Z, Gu S, Fang G, Liu Y, Luo Y, Liu H, Zhang T, et al. Purified CD34(+) cells versus peripheral blood mononuclear cells in the treatment of angiitis-induced no-option critical limb ischaemia: 12-Month results of a prospective randomised single-blinded non-inferiority trial. EBioMedicine. 2018;35:46–57.
31. Cacione DG, do Carmo Novaes F, Moreno DH. Stem cell therapy for treatment of thromboangiitis obliterans (Buerger's disease). Cochrane Database Syst Rev. 2018;10:Cd012794.
32. Martín-González C, Pelazas-González R, Fernández-Rodríguez C, Alemán-Valls R, Martínez-Riera A, Ortega-Toledo P, García-Rodríguez A, Rodríguez-Gaspar M, González-Reimers E. Ferritin and liver fibrosis among patients with chronic hepatitis C virus infection. J Trace Elem Med Biol. 2020;61:126542.
33. Fazeli B, Ligi D, Keramat S, Maniscalco R, Sharebiani H, Mannello F. Recent updates and advances in winiwarter-buerger disease (thromboangiitis obliterans): biomolecular mechanisms, diagnostics and clinical consequences. Diagnostics (Basel, Switzerland). 2021;11:1736.
34. Arslan C, Altan H, Beşirli K, Aydemir B, Kiziler AR, Denli S. The role of oxidative stress and antioxidant defenses in buerger disease and atherosclerotic peripheral arterial occlusive disease. Ann Vasc Surg. 2010;24:455–60.
35. Feng H, Schorpp K, Jin J, Yozwiak CE, Hoffstrom BG, Decker AM, Rajbhandari P, Stokes ME, Bender HG, Csuka JM, et al. Transferrin receptor is a specific ferroptosis marker. Cell Rep. 2020;30:3411-3423.e3417.
36. Liao P, Wang W, Wang W, Kryczek I, Li X, Bian Y, Sell A, Wei S, Grove S, Johnson JK, et al. CD8(+) T cells and fatty acids orchestrate tumor ferroptosis and immunity via ACSL4. Cancer Cell. 2022;40:365-378.e366.
37. Wu J, Minikes AM, Gao M, Bian H, Li Y, Stockwell BR, Chen ZN, Jiang X. Intercellular interaction dictates cancer cell ferroptosis via NF2-YAP signalling. Nature. 2019;572:402–6.
38. Feng J, Guo J, Wang JP, Chai BF. MiR-32-5p aggravates intestinal epithelial cell injury in pediatric enteritis induced by Helicobacter pylori. World J Gastroenterol. 2019;25:6222–37.
39. Zhang P, Luo J, Wu T, Wang X, Yang F, Yu Y, Lu L, Yu H. MiR-32-5p/AIDA mediates OxLDL-induced endothelial injury and inflammation. Int Heart J. 2022;63:928–38.
40. Liu YJ, Zhou HG, Chen LH, Qu DC, Wang CJ, Xia ZY, Zheng JH. MiR-32-5p regulates the proliferation and metastasis of cervical cancer cells by targeting HOXB8. Eur Rev Med Pharmacol Sci. 2019;23:87–95.

Publisher's Note